A Novel Strategy for Constructing Ecological Index of Tea Plantations Integrating Remote Sensing and Environmental Data

Yilin Mao, He Li, Yu Wang, Yang Xu, Kai Fan, Jiazhi Shen, Xiao Han, Qingping Ma, Hongtao Shi, Caihong Bi, Yunlai Feng, Zhaotang Ding, and Litao Sun

***Abstract*—The structure of plant communities and their response to temperature variations are an essential basis for evaluating the ecological structure and function of tea plantations. However, field surveys and quantitative evaluation of plant communities and ecotea plantations remain challenging. In this study, a novel strategy was proposed for rapid surveillance of plant community structure and its response to changes in weather conditions in tea plantations. This strategy aims to construct the normalized tea plantation ecological index (NTEI) by synergizing environmental parameters with multisource remote sensing data; establish the fitting and inversion model of NTEI by cascading the Fourier function with the convolutional neural networks gate recurrent unit (CNN-GRU) network; and evaluate the variability of the plant community in tea plantations by analyzing the variation characteristics of the NTEI and the measured temperature. The study revealed the following: First, the NTEI can objectively characterize the plant communities of tea plantations, and its variation characteristics were consistent with the changes in vegetation phenology and temperature; second, the Fourier function has the potential to quantify NTEI, and it is fitting R^2 for the NTEI of nine plant communities ranged from 0.840 to 0.921; third, the CNN-GRU has the most advantage in establishing the prediction model of NTEI, and its prediction accuracy was $Rp^2 = 0.955$ and RMSEP $= 0.314$; and fourth, the plant communities with high species richness increased regional ecological stability, had a strong buffering capacity against temperature changes, and had less variability in NTEI. The results provide significant guidance for building plant community structures and improving the ecological benefits of tea plantations.**

***Index Terms*—Convolutional neural networks gate recurrent unit (CNN-GRU), ecological tea plantation, environmental parameters, multisource remote sensing, plant community, UAV.**

I. Introduction

ECOLOGICAL tea plantation is a composite ecosystem paradigm with the tea plant (*Camellia sinensis* (L.) O. Kuntze.) as the main species, which is in line with the biological characteristics of the tea plant that is fond of temperature and humidity, and suitable for scattered light, and at the same time follows the natural law of ecological balance [1]. In the specific ecosystem of a tea plantation, the ecological status is a complex and multidimensional system that encompasses environmental factors, such as air humiture, soil temperature and moisture, and illumination, while also incorporating biological factors, such as biodiversity and plant community structure, and emphasizing the dynamic balance among them. In order to maintain this balance, people have constructed ecological tea plantations with different plant community structures based on the generic pattern of ecological tea plantations and their own subjective ideas [2]. It is expected that this measure will effectively alleviate the adverse effects of high or low temperatures and droughts on tea plants in the North Yangtze District of China. However, the ecological status of these tea plantations is difficult to measure quantitatively, which affects the standardization of ecological tea plantation construction. How to reveal the differences in the community structure of different tea plantations and their influence on the stability of tea plantation ecosystems has become an important issue to be solved at this stage.

The plant community structure and its response to weather conditions change is an essential basis for monitoring and evaluating the ecological structure and functions of tea plantations. The traditional methods of monitoring and evaluating vegetation usually involve direct observations of key indicators, such as plant type, crown width, plant height, and leaf area, through field surveys. This field survey method, while able to provide researchers with intuitive and detailed data support, also has limitations in practical operations, such as requiring a great

Manuscript received 8 February 2024; revised 28 May 2024; accepted 26 June 2024. Date of publication 5 July 2024; date of current version 24 July 2024. This work was supported in part by the Innovation Project of Shandong Academy of Agricultural Sciences under Grant CXGC2023F18 and Grant CXGC2023A11, in part by Rizhao Science and Technology Innovation Project under Grant 2020cxzx1104, in part by the Technology System of Modern Agricultural Industry in Shandong Province under Grant SDAIT-19-01, in part by the Special Foundation for Distinguished Taishan Scholar of Shandong Province under Grant ts201712057, and in part by the Natural Science Foundation of Shandong Province under Grant ZR2023QC086. *(Yilin Mao and He Li are co-first authors.) (Corresponding authors: Zhaotang Ding; Litao Sun.)*

Yilin Mao, He Li, Jiazhi Shen, Zhaotang Ding, and Litao Sun are with the Tea Research Institute, Shandong Academy of Agricultural Sciences, Jinan 250100, China (e-mail: maoyilintea@163.com; lihetea@163.com; shenjiazhitea@163.com; dzttea@163.com; slttea@163.com).

Yu Wang, Yang Xu, Kai Fan, and Xiao Han are with the College of Horticulture, Qingdao Agricultural University, Qingdao 266109, China (e-mail: wangyutea@163.com; xuyangtea99@163.com; fankaitea@163.com; hanxiao1342@163.com).

Qingping Ma is with the College of Agronomy, Liaocheng University, Liaocheng 252000, China (e-mail: maqingpingtea@163.com).

Hongtao Shi is with the School of Science and Information Science, Qingdao Agricultural University, Qingdao 266109, China (e-mail: sht@qau.edu.cn).

Caihong Bi is with the Agricultural Technology Extension Center, Linyi Agricultural and Rural Bureau, Linyi 276037, China (e-mail: caihongbi@126.com).

Yunlai Feng is with the Chunxi Tea Industry Company Limited of Shandong, Linyi 276000, China (e-mail: chunxitea@163.com).

Digital Object Identifier 10.1109/JSTARS.2024.3424200

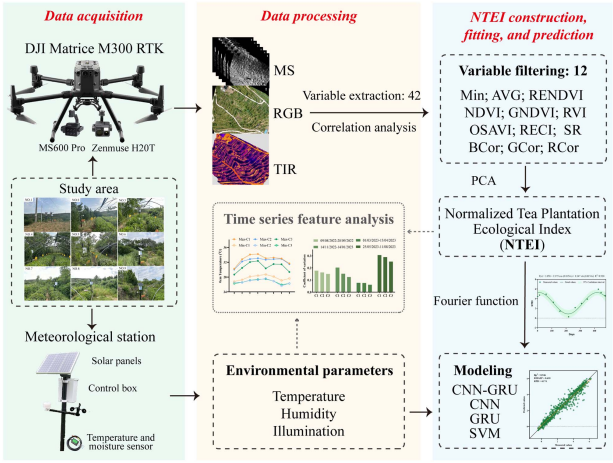

Fig. 1. Data collection, processing, and analyzing process of this study.

deal of manpower and material resources, as well as consuming a considerable amount of time when conducting large-scale investigations [3].

Remote sensing technology, with its efficient, unbiased, and dynamic quantitative monitoring characteristics, has gradually become the most effective and practical method for regional or global ecological evaluation [4], [5]. Currently, scholars from various countries have utilized remote sensing indices based on satellite data to monitor changes in large-scale ecosystems, including individual indices, such as global water index based on Landsat [6], normalized difference vegetation index (NDVI) [7], and enhanced vegetation index (EVI) [8] based on MODIS, as well as composite indices, such as remote sensing based ecological index (RSEI) [9] and ecological risk index [10] based on Landsat. However, due to the low spatial and temporal resolution of satellite remote sensing data, these indices are often only applicable to ecosystems, such as forests and cities, making it difficult to adequately reflect the ecological status of small-scale plantations, especially in evaluating the impact of multiple plant communities on ecosystems [11], [12]. The data collected by UAVs, characterized by high precision and high resolution, provide a new opportunity for refined ecological monitoring of tea plantations. In recent years, the significant advantages of UAVs in the monitoring of tea plantation ecosystems have been demonstrated by our team. On the one hand, their high maneuverability and flexibility enable the UAV to quickly cover a wide area of tea plantations, thus enabling the monitoring of the growth conditions of tea plants and intercrops [13]. On the other hand, the multispectral (MS) and visible light sensors carried by the UAV can capture multidimensional information about the tea plantations, including key parameters, such as the health of the tea plants and the quality of the tea leaves. This information is crucial for accurately assessing the status of tea plantations and optimizing tea plantation management strategies [14], [15].

Meanwhile, environmental data are also crucial for ecological monitoring. More and more scholars have combined continuous observation data from meteorological stations, with remote sensing data for ecological evaluation research. For example, Zhong et al. [16] investigated the response of vegetation to drought using multiple remote sensing and meteorological indicators from 48 states in the United States; Leng et al. [17] developed a practical method for all-weather soil moisture acquisition by combining optical/thermal infrared (TIR) information from satellite images and gridded meteorological products. Recently, in the direction of synergizing environmental data and spectral data, our laboratory has also made some explorations. By synergizing meteorological station data (temperature, humidity, and illuminance) and hyperspectral data, and combining them with deep learning algorithms, a dynamic model of tea seedling growth was established [18]. Previous study has synergized and analyzed heterogeneous data from multiple sources and realized the monitoring of agronomic parameters of tea plants. This lays the foundation for this work to synergize environmental and remote sensing data in order to probe the ecological status of tea plantations.

Based on the above analysis, in this work, a deep learning network was used to conduct collaborative research on environmental data and multisource remote sensing data, and a "Space–Earth" integrated monitoring mode was established, in order to realize timely, accurate, and continuous monitoring of the ecological status of tea plantations. The graphical abstract is shown in Fig. 1. The experimental site was in the Chunxi Tea Plantation in Shandong Province, China, of which nine plant communities were selected for the study. Temperature, humidity, and illuminance data were obtained continuously by using the environmental monitoring system of the meteorological station, and MS, visible (RGB), and TIR data by using the multisource remote sensing system of the UAV; a normalized tea plantation ecological index (NTEI) was constructed for monitoring the ecological status of tea plantations; and NTEI fitting model based on Fourier function and NTEI prediction model based on convolution neural network (CNN), gate recurrent unit (GRU), CNN-GRU, and support vector machine (SVM) were established. In addition, during periods of acute fluctuations in air temperature, the responses of the maximum and minimum temperature in different plant communities, as well as the variability and fluctuation of their NTEIs, were compared. The effects of diverse plant communities on the ecological stability of tea plantations were explored. This study is the first to synergistically process and analyze temperature, humidity, and illumination data, as well as the remote sensing index. Then, the Fourier model and machine learning model are cascaded and coupled to fit and predict the NTEI values, thereby determining the vegetation phenological changes and ecological status of tea plantations. This provides an objective, rapid, and effective new strategy for plant community monitoring of tea plantations, which has great significance as a guide to carrying out the construction of plant communities and the enhancement of ecological benefits in northern tea plantations.

II. Materials and Methods

A. Experimental Area

1) Overview of the Experimental Area: The experimental area was Chunxi Tea Plantation [see Fig. 2(a)] (117.45°E, 35.11°N), located in Linyi City, Shandong Province, China,

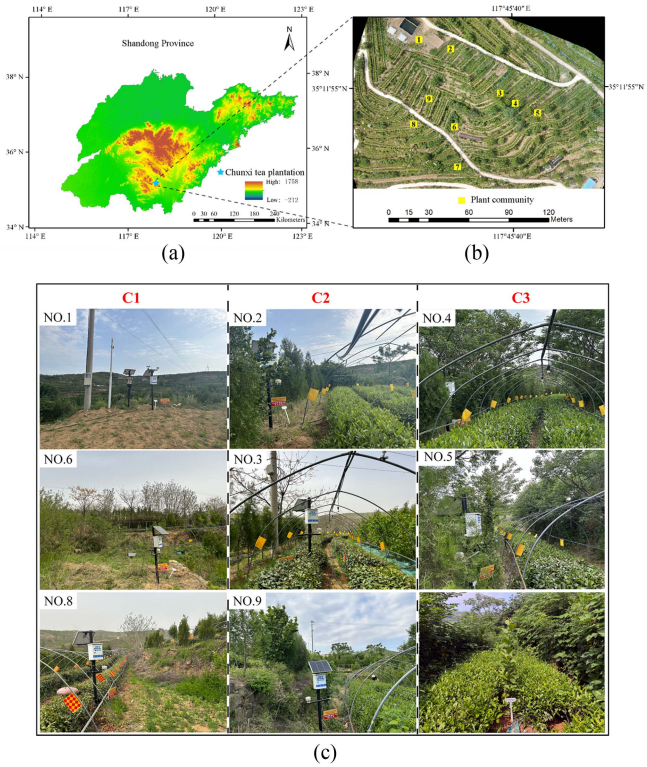

Fig. 2. Location of the experimental area and the plant communities. (a) Labeled locations of the Chunxi Tea Plantation, Shandong Province, China. (b) Marked locations of the nine plant communities. (c) Displayed details of the nine plant communities.

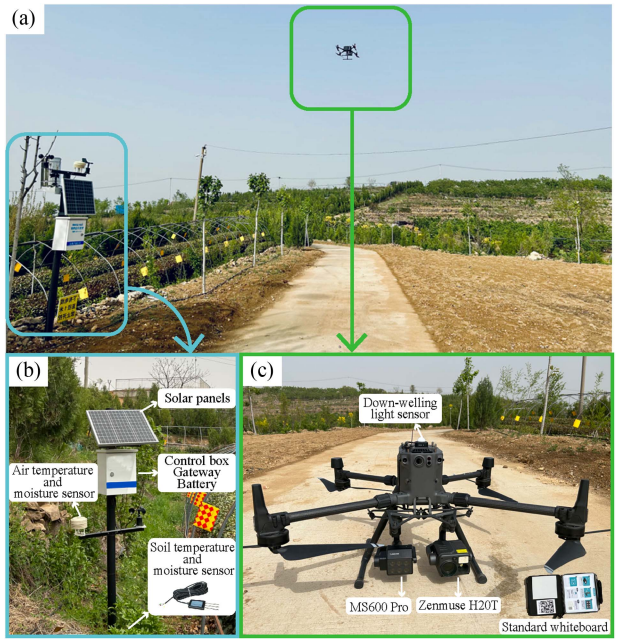

Fig. 3. Data acquisition. (a) Research data sources. (b) Meteorological station monitoring system. (c) UAV multisource remote sensing system.

which belongs to the North Yangtze District of China. The climate of the area is a temperate continental monsoon climate, which is characterized by four distinctive seasons. Summer is warm and humid, and disasters weather, such as floods, high temperatures, and droughts, are more frequent; Winter is cold and dry, and catastrophic weather, such as cold snaps and late frosts, can occur from time-to-time. From August 2022 to August 2023, the average annual temperature was 9 °C, with an extreme annual high temperature of 38 °C and an extreme annual low temperature of −11 °C; and the total rainfall was 824.1 mm.

The Chunxi Tea Plantation occupies a total area of 155 acres, with an elevation of 483 m and a terraced terrain. It is an artificial composite tea plantation ecosystem, which is the product of the combination of natural geography and artificial transformation. There are a large number of plant species in the tea plantation. Besides the main crop, the tea plant, the dominant species include neem (*Melia azedarach* L.), paper mulberry (*Broussonetia papyrifera* L.), mulberry (*Morus alba* L.), mugwort (*Artemisia argyi* H.), and horseweed (*Erigeron canadensis* L.). The later artificial plantings also comprise lateral oriental arborvitae (*Platycladus orientalis* L.), hazelnut (*Corylus heterophylla* Fisch.), honeysuckle (*Lonicera japonica* Thunb.), vetch (*Vicia sepium* L.), and so on.

2) Characterization of Plant Communities: To characterize the distribution and structure of plant communities in the tea plantation, a UAV was first used for field surveys to locate different plant cover densities, which were combined with ground observations. The nine different kinds of plant communities were selected as the basic types of plant communities for the research of Chunxi Tea Plantation. Finally, according to the survey routes, the nine plant communities were numbered as NO.1, NO.2, …, and NO.9 [see Fig. 2(b) and (c)].

The field investigation was carried out during the vigorous growth period of plants (May–August 2022 and May–August 2023). Each plant community was located using the global positioning system and the sample methods (5 m × 5 m) were used to comprehensively survey the basic characteristics of the nine plant communities, including species name, abundance, and height. The basic vegetation characteristics of the nine plant communities are shown in Table I.

Based on the species abundance and community α-diversity (Simpson index), the nine plant communities were classified into three categories. Category 1 (C1): NO.1, NO.6, and NO.8, $0 \leq$Richness<4, $0 \leq$Simpson<0.4. Category 2 (C2): NO.2, NO.3, and NO.9, $4 \leq$Richness<7, $0.4 \leq$Simpson<0.7. Category 3 (C3): NO.4, NO.5, and NO.7, $8 \leq$Richness<10, $0.7 \leq$Simpson<1.0.

B. Data Acquisition

The research data in this article were mainly divided into two parts (see Fig. 3). One part was the environmental sensing data generated by multiple sensors in the meteorological station monitoring system. It included air temperature and humidity, soil temperature and humidity, and illuminance. It was primarily used to characterize the weather conditions change and stability of the tea plantation ecosystem. The other part was multisource remote sensing data collected by low-altitude UAV, including MS, RGB, and TIR data. It was mainly used to characterize the vegetation and ecological status of tea plantations.

TABLE I
VEGETATION CHARACTERISTICS OF THE NINE PLANT COMMUNITIES

NO.	Coordinates (N, E)	Richness	Dominant species	Abundance (plants/m^2)	Average height	Simpson
1	35.19889722°, 117.76040000°	-	-	-	-	0.000
2	35.19887500°, 117.76057222°	4	Tea plants (*Camellia sinensis* L.)	6.0	0.8	0.489
			Oriental arborvitae (*Platycladus orientalis* L.)	0.6	2.4	
			Hazelnut (*Corylus heterophylla* Fisch.)	0.2	2.0	
			Crabgrass (*Digitaria sanguinalis* L.)	2.0	0.1	
3	35.19857778°, 117.76099722°	6	Tea plants (*Camellia sinensis* L.)	6.0	0.8	0.679
			Oriental arborvitae (*Platycladus orientalis* L.)	1.2	2.2	
			Neem (*Melia azedarach* L.)	0.6	3.2	
			Hazelnut (*Corylus heterophylla* Fisch.)	1.0	1.4	
			Dayflower (*Commelina communis* L.)	1.4	0.1	
			Horseweed (*Erigeron canadensis* L.)	1.0	0.2	
4	35.19849444°, 117.76106944°	9	Tea plants (*Camellia sinensis* L.)	6.0	0.8	0.813
			Oriental arborvitae (*Platycladus orientalis* L.)	0.6	2.1	
			Neem (*Melia azedarach* L.)	0.6	3.6	
			Hazelnut (*Corylus heterophylla* Fisch.)	0.2	1.9	
			Dayflower (*Commelina communis* L.)	2.6	0.1	
			Scandent hop (*Humulus scandens* Lour.)	0.8	1.2	
			Horseweed (*Erigeron canadensis* L.)	1.2	0.3	
			Morning glory (*Calystegia hederacea* Wall.)	3.0	0.1	
			Mugwort (*Artemisia argyi* H.)	3.2	0.4	
5	35.19842778°, 117.76118056°	9	Tea plants (*Camellia sinensis* L.)	4.0	0.8	0.798
			Oriental arborvitae (*Platycladus orientalis* L.)	0.6	2.2	
			Neem (*Melia azedarach* L.)	0.2	3.5	
			Hazelnut (*Corylus heterophylla* Fisch.)	0.2	1.9	
			Crabgrass (*Digitaria sanguinalis* L.)	0.8	0.2	
			Scandent hop (*Humulus scandens* Lour.)	0.8	1.0	
			Horseweed (*Erigeron canadensis* L.)	2.4	0.2	
			Morning glory (*Calystegia hederacea* Wall.)	6.0	0.1	
			Poke root（*Phytolacca acinosa* Roxb）	3.0	0.4	
6	35.19837222°, 117.76066667°	1	Mugwort (*Artemisia argyi* H.)	10.0	0.6	0.000
7	35.19816667°, 117.76068333°	8	Tea plants (*Camellia sinensis* L.)	6.0	0.7	0.775
			Paper mulberry (*Broussonetia papyrifera L.*)	0.2	2.3	
			Neem (*Melia azedarach* L.)	0.4	1.4	
			Elm (*Ulmus pumila* L.)	0.2	1.9	
			Locust (*Robinia pseudoacacia* L.)	0.4	2.1	
			Crabgrass (*Digitaria sanguinalis* L.)	4.0	0.2	
			Horseweed (*Erigeron canadensis* L.)	3.0	0.1	
			Morning glory (*Calystegia hederacea* Wall.)	4.0	0.3	
8	35.19816944°, 117.76068611°	2	Tea plants (*Camellia sinensis* L.)	4.0	0.8	0.385
			Crabgrass (*Digitaria sanguinalis* L.)	5.0	0.2	
9	35.19855278°, 117.76049444°	5	Tea plants (*Camellia sinensis* L.)	6.0	0.8	0.475
			Oriental arborvitae (*Platycladus orientalis* L.)	1.0	2.3	
			Hazelnut (*Corylus heterophylla* Fisch.)	0.4	1.7	
			Wiregrass (*Eleusine indica* L.)	0.8	0.3	
			Scandent hop (*Humulus scandens* Lour.)	0.2	0.5	

1) Acquisition of Environmental Data: The environmental monitoring system [see Fig. 3(b)] of the meteorological station (Kerun Information Technology Co., Ltd., Shandong, China) was utilized to obtain the environmental data. The meteorological station in the tea plantation was installed on 9 August 2022, and consists of three main components.

i) Perception layer: It mainly consisted of temperature, humidity, and illumination sensors, which were installed in the center of each plant community. The temperature and humidity sensors were installed in four layers, including 100 cm above ground (100 cm), 0 cm above ground (0 cm), 20 cm below ground (−20 cm), and 40 cm below ground (−40 cm); and illuminance sensors were installed one layer at 100 cm above ground. These sensors were powered by solar energy and had a data acquisition cycle of every 30 min, capable of accumulating 48 data points (24 h × 60 min/h/30 min/times = 48) every day.

ii) Network layer: It was mainly responsible for receiving the data recorded by the sensors and transmitting them to servers through 4G networks.

iii) Application layer: It mainly implemented the query and processing of sensor data, and finally realized data viewing and

TABLE II
BAND PARAMETERS AND CHARACTERISTICS OF MS600 PRO

Wavelength	Color	Center (nm)	Bandwidth (nm)
Blue	blue	452	35
Green	green	555	25
Red	red	660	20
Red edge	pink	720	10
Red edge	deep pink	750	15
Near infrared	lavender	840	35

sharing in the form of webpage[1] and WeChat applet (Farmer's Treasure).

In order to make the data suitable for the analysis in this work, all raw environmental data from 9 August 2022 to 30 September 2023 were exported to Excel, a total of 418 days. Subsequently, the average, maximum, and minimum values of the 48 data points for each day were calculated, which will be utilized for further analysis.

2) Acquisition of Remote Sensing Data: The low-altitude UAV platform [see Fig. 3(c)] was utilized to acquire multisource and multitemporal remote sensing data. The UAV flight platform was a DJI Matrice M300 RTK (DJI Co., Ltd., Shenzhen, China), equipped with a dual cloud platform carrying the MS600 Pro (Yusense Co., Ltd., Qingdao, China) and the Zenmuse H20T (DJI Co., Ltd., Shenzhen, China).

The MS600 Pro is a customized MS sensor for acquiring MS data in six bands. The specific bands and their characteristics are shown in Table II. The MS sensor has a complementary metal–oxide–semiconductor (CMOS) sensor with a target size of 1/3". The pixels are 1.2 million, the shutter type is global, the field of view is 49.5°×38.1° (horizontal × vertical), the capture mode is overlapping rate triggered (forward: 80% and lateral: 70%), and the image format is TIFF. In this study, the effect of light on MS data acquisition was reduced by standard gray plate calibration and downlink light sensor (DLS) correction, which ensured the authenticity of feature spectral reflectance. Before each flight, images of the standard gray plate were taken and were used in the radiation calibration process of MS data in the later stage. During the flight, the DLS mounted horizontally on top of the UAV synchronously measured the ambient light corresponding to the six bands and recorded it in the metadata of the captured images, which was used to automatically calibrate the light changes.

The Zenmuse H20T is equipped with a visible light sensor and a thermal imaging sensor for obtaining RGB and TIR data, respectively. The RGB sensor has a CMOS sensor with a target size of 1/1.7". The pixels are 20 million, the shutter type is rolling, the field of view is 66.6° (Display), the shooting mode is timed trigger (2 s), and the image format is JEPG. The type of thermal imaging sensor is an uncooled vanadium oxide microbolometer. The resolution is 640×512, the field of view is 40.6° (Display), the capture mode is timed triggered (2 s), and the image format is R-JEPG.

[1][Online]. Available: https://kr.miots.cn/login

In order to mitigate the adverse effects of weather conditions on remote sensing data, the on-site UAV operation was carried out in sunny weather with good light conditions and low wind speed. The flight time was 11:00–14:00 noon, the flight altitude was 30 m, and the flight speed was 2.5 m/s. The specific flight dates were 11 June ($x1$, indicating the number of days the test was conducted, with this date as the first day), 24 June, 9 August, 28 September, and 14 November in 2022, and 14 January, 1 March, 15 April, 25 May, 11 August, 30 August, and 27 September in 2023. A total of 12 flight tests were conducted with intervals of 13d, 46d, 50d, 47d, 61d, 46d, 45d, 40d, 78d, 19d, and 28d, respectively.

C. Data Analysis

1) Extraction of Remote Sensing Variables: In order to make the remote sensing data suitable for further processing and analysis, the raw MS, RGB, and TIR images were first preprocessed using Yusense Map (V1.0) software. Through the processes of band alignment, radiometric calibration, and image stitching, the original and single MS images were output as a complete MS image of the experimental area. Through processes, such as camera parameter generation and temperature normalization, the original RGB and TIR images were output as RGB and TIR images of the study area. After that, spectral information, structural information, and temperature information were extracted from the MS, RGB, and TIR images, respectively.

Extraction of spectral information: In the remote sensing processing software ENVI (V5.3) (Research System, Inc., America), the mean spectral reflectance of each community was extracted from the MS images using the region of interest (ROI) tool. The mean spectral reflectance was obtained by calculating the average value of the spectral reflectance of all pixels within the ROI in each band. Then, referring to the existing research results [19], 15 common vegetation indices were calculated according to the formulae, as listed in Table III. Therefore, the initial spectral information dataset of this study consists of 6+15 = 21 variables.

Extraction of structural information: In the ENVI (V5.3), three-channel texture information was extracted from the RGB image for each community using the cooccurrence measures tool. The texture information type was an 8-D grayscale cooccurrence matrix, including mean (Mean), variance (Var), homogeneity (Hom), contrast (Con), disparity (Dis), entropy (Ent), second-order moment (SM), and correlation (Cor) [31]. Therefore, the initial structural information dataset for this study consists of $3 \times 8 = 24$ variables.

Extraction of temperature information: In the DJI thermal analysis tool (V3.0) (DJI Co., Ltd., China) software, the maximum temperature (Max), the minimum temperature (Min), and the average temperature (AVG) of each community were extracted from the TIR images using the rectangular thermometry tool. Therefore, the initial temperature information dataset for this study consisted of three variables.

2) Construction and Fitting of NTEIs: Construction of NTEI: To better characterize the stability of ecological tea plantations, remote sensing variables that were sensitive to changes in the

TABLE III
FULL TITLE AND CALCULATION FORMULA OF 15 VEGETATION INDICES

Spectral parameters	Full title	Formula	References
DVI	Difference vegetation index	NIR.840-G.555	[20]
NDVI	Normalized difference vegetation index	(NIR.840-R.660)/(NIR.840+R.660)	[21]
EVI	Enhanced vegetation index	2.5*(NIR.840-G.555)/(NIR.840+6*R.660-7.5B.450+1)	[22]
GNDVI	Green-normalized difference vegetation index	(NIR.840-G.555)/(NIR.840+G.555)	[23]
PPR	Plant pigment ratio	(G.555-B.450)/(G.555+B.450)	[24]
SIPI	Structure-insensitive pigment index	(NIR.840-B.450)/(NIR.940-R.660)	[25]
RECI	Red-edge chlorophyll index	NIR.840/RE.710-1	[26]
RENDVI	Red-edge NDVI	(NIR.940-RE.710)/(NIR.940+RE.710)	[26]
MCARI	Modified chlorophyll absorption ratio index	(RE.710-R.660-0.2(RE.710-R.660))* (RE.710/R.660)	[27]
TCARI	Transformed chlorophyll absorption reflectance index	3*((RE710-R.660)-0.2*(RE.710-G.555)*(RE.710/G.555))	[27]
OSAVI	Optimization of soil-adjusted vegetation index	1.16*(NIR.840-R.660)/(NIR.840+R.660+0.16)	[28]
RVI	Ratio vegetation index	NIR.840/R.660	[26]
SAVI	Soil-adjusted vegetation index	(NIR.840-R.660)/(NIR.840+R.660+0.5)	[29]
SR	Simple ratio vegetation index	RE.750/G.555	[30]
RDVI	Renormalized difference vegetation index	(NIR.840-R.660)/(NIR.840+R.660)1/2	[21]

microclimate of plant communities were identified. The correlations of 21 spectral, 24 structural, and 3 temperature variables with the environmental data (air humiture, soil humiture, and illuminance) of the tea plantations were analyzed with the SPSS software. Using principal component analysis (PCA), remote sensing variables highly correlated with temperature, humidity, and illumination were constructed into NTEI sensitive to the ecological status of tea plantations. Based on the methods mentioned in the previous articles of the research group, the raw data were first standardized and then subjected to PCA [32]. Specifically, in SPSS software, the "dimensionality reduction" tool was utilized to perform principal component operations to determine the initial eigenvalues [including eigenvalue (λ), variance contribution (VC) rate, and cumulative variance contribution (CVC) rate] and loading coefficients (LCs) of each principal component. Then, the first n principal components, whose eigenvalues are greater than 1, were selected and used in the construction of the NTEI. Next, the linear combination coefficients (LCCs) and composite score coefficients (CSCs) were calculated using (1) and (2), respectively. Finally, the calculation formula for NTEI was obtained based on the percentage method. The simplified expression of NTEI is presented in (3)

$$\mathrm{LCC}_{ij} = \frac{\mathrm{LC}_{ij}}{\sqrt{\lambda_j}} \tag{1}$$

$$\mathrm{CSC}_i = \sum_{i=1}^{n} \frac{\mathrm{LCC} \times \mathrm{VC}}{\mathrm{CVC}} \tag{2}$$

$$\mathrm{NTEI} = \sum_{i=1}^{m} \frac{\mathrm{CSC}_i}{\sum_{i=1}^{m} \mathrm{CSC}_i} \times X_i. \tag{3}$$

In (1), LC_{ij} is the loading coefficient of the jth principal component and ith indicator, and λ_i is the eigenvalue of jth. In (2), n is the number of principal components involved in the construction of NTEI. In (3), X_i is the ith remote sensing variable, and m is the number of remote sensing variables participating in PCA.

Fitting of NTEI variation curves: The Fourier fitting function is a very effective analytical method for dealing with periodic data. In order to reconstruct the NTEI data of a continuous time series, the Fourier function was used to fit the NTEI with a periodic regularity and to quantify the variation curve of the NTEI (operating environment: MATLAB 2020). The initial date of the NTEI quantization curve was 11 June 2022, and the end date was 30 September 2023, for a total of 477 days. To enhance the computational efficiency, in this study, the selected Fourier expansion level was 1, and its fitting function was expressed as follows:

$$f\ (x) = a_0\ + a\cos(wx) + b\sin(wx). \tag{4}$$

In (4), x is the number of days from the initial date of the experiment (e.g., 11 June 2022, $x = 1$), and a_0, a, b, and w are the constants.

The sum of squares due to error (SSE), coefficient of determination (R^2), degree-of-freedom adjusted R^2 (Adj.R^2), and root-mean-square error (RMSE) were chosen to evaluate the effectiveness of Fourier's fit to the NTEI. Among them, SSE and RMSE were smaller and closer to 0, showing the stronger performance of the model. R^2 and Adj.R^2 were larger and closer to 1, indicating a better fitting of the data. Their specific formulae were given as follows:

$$\mathrm{SSE} = \sum_{i=1}^{n} (y_i - \hat{y}_i)^2 \tag{5}$$

$$R^2 = 1 - \frac{\sum_{i=1}^{n} (y_i - \hat{y}_i)^2}{\sum_{i=1}^{n} (y_i - \bar{y})^2} \tag{6}$$

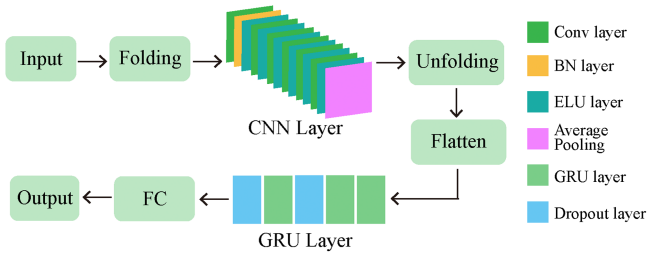

Fig. 4. CNN-GRU network architecture. Conv: convolution; BN: batch normalization; ELU: exponential linear unit (activation function); and FC: fully connected.

$$\text{Adj. } R^2 = 1 - \frac{\left(1 - R^2\right)(n-1)}{n-p-1} \tag{7}$$

$$\text{RMSE} = \sqrt{\frac{\sum_{i=1}^{n}\left(y_i - \hat{y}_i\right)^2}{n}}. \tag{8}$$

In (5)–(8), n is the number of NTEI data, y_i is the true value of NTEI, $\hat{y}_i$ is the fitted value of NTEI, $\bar{y}$ is the average true value of NTEI, and p is the number of features.

3) Prediction of NTEIs: In order to synergize the environmental data with the remote sensing data, regression models were developed between the environmental data of different communities and their NTEI data to predict future NTEI. NTEI data from 9 August 2022 to 30 September 2023 were selected, for a total of 418 days. They were used in the NTEI modeling process to better match environmental data. Therefore, in this study, the NTEI dataset and the humiture and illumination dataset for the nine plant communities contained $418 \times 9 = 3762$ data. Simultaneously, according to the 3:1 rule, the total dataset was divided into a training set (2821 samples) and a testing set (941 samples), which were utilized for the training and testing of the NTEI regression model, respectively. In order to synergize the environmental data with the remote sensing data, a regression model was developed between the environmental data and NTEI data of different plant communities using a hybrid CNN-GRU network to predict NTEI (operating environment: MATLAB 2020). The structure of the hybrid CNN-GRU network is shown in Fig. 4, which includes a CNN network with strong feature extraction capability and a GRU network that is good at exploiting time-series data. In addition, to further validate the performance of the CNN-GRU, several regression models were built using CNN, GRU, and SVM, and the results were compared with those of CNN-GRU. The specific parameters of CNN-GRU, CNN, GRU, and SVM networks are shown in Table IV.

Six metrics were selected to evaluate the predictive effectiveness of the model for NTEI. These include RMSE (7) for validation (RMSECV), calibration (RMSEC), and prediction (RMSEP), and R^2 (5) for calibration (Rc^2) and prediction (Rp^2). Among them, the smaller the RMSECV, RMSEC, and RMSEP, the larger the Rc^2 and Rp^2, indicating better performance of the model.

TABLE IV
MAIN PARAMETERS OF THE CNN-GRU, CNN, GRU, AND SVM MODELS

Model	Model parameters	Value
CNN-GRU	Normalize	L2
	Optimizer	Adam (Adaptive moment estimation)
	Activation Function	ELU (Exponential Linear Unit)
	Batch Size	32
	Learning Rate	0.001
	Epochs	100
	Dropout	0.5
	Verbose	1
CNN	Normalize	L2
	Optimizer	Adam
	The Activation Function	ELU
	Batch Size	32
	Learning Rate	0.001
	Epochs	100
	Dropout	0.5
	Verbose	1
GRU	Normalize	L2
	Optimizer	Adam
	Activation Function	Tanh (TanHyperbolic)
	Num of Hidden Units	20
	Batch Size	32
	Learning Rate	0.001
	Epochs	150
	Dropout	0.5
	Verbose	1
SVM	The Kernel Function	Polynomial Kernel
	Cache_size	200
	Tol (Tolerance Used in the Iterative Algorithm)	10^{-3}
	Max_iter	−1
	C (Regularization Parameter)	1

III. RESULTS

A. Analysis of Temperatures at the Center Site of Different Plant Communities

1) Spatiotemporal Variations in Temperature of Three Plant Community Categories: Temperature is a key factor affecting vegetation phenology. In order to investigate the temporal and spatial variation patterns of temperature at different plant communities, the interannual variation curves of daily mean temperature at the 100, 0, −20, and −40 cm layers of three plant community categories were plotted from 9 August 2022 to 30 September 2023 [see Fig. 5(a)]. It can be seen that the temperature varies significantly with the change of seasons, with the lowest peak of temperature occurring in winter. In winter, the −20 and −40 cm layers of C1, C2, and C3 were consistently above 0 °C, while the 100 cm layer was frequently below 0 °C. The difference was that the temperature of the 0 cm layer of C1 was close to or below 0 °C, whereas the temperature of the 0 cm layer of C2 and C3 was able to maintain above 0 °C all the time. As a result, C2 and C3 were responsible for providing relatively high-temperature conditions for the tea plant during the severe winter.

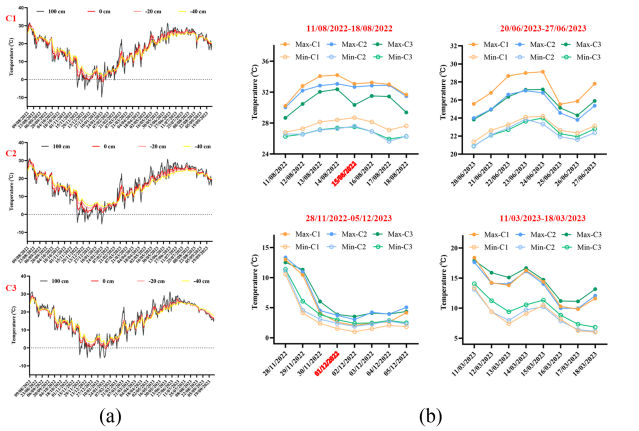

Fig. 5. Response of three categories of plant communities to temperature changes. (a) Interannual variation curves of temperature at different layers. (b) 0 cm max/min temperature response to external high/low temperatures.

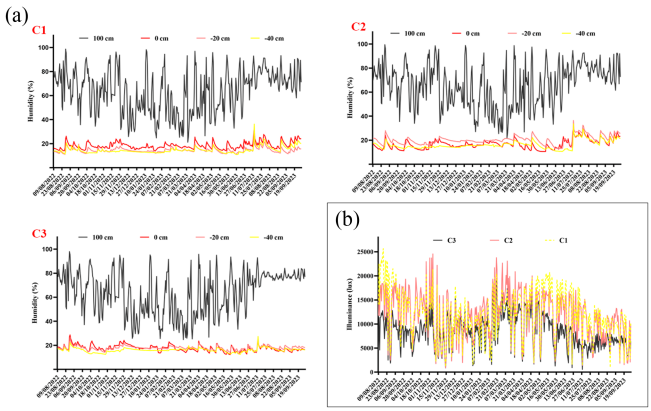

Fig. 6. Variations of humidity and illuminance at different layers of three categories of plant communities. (a) Interannual variation curves of humidity at different layers. (b) Interannual variation curves of illuminance at different layers.

The four-layer temperatures of the three categories of plant communities generally showed a decreasing and then increasing trend, fluctuating within the range of −10 °C–33 °C. Specifically, the magnitude of change in air temperature at 100 cm was significantly higher than the variation in soil temperature at 0, −20, and −40 cm. In soil temperature, the deeper the soil, the smaller the variation. The temperatures at 0 cm were relatively more variable, while the temperatures at −40 cm were the least variable. For example, at the lowest peak of winter temperatures, the temperature at 0 cm was relatively lowest, close to 0 °C; the temperature at −20 cm was next highest; and the temperature at −40 cm was relatively highest. This was because the temperature at 0 cm was strongly influenced by air temperature, while temperature transfer in the soil was slower. Therefore, the closer to the surface, the lower the temperature.

Additionally, the interannual variation curves of humidity and illuminance for different categories of plant communities are shown in Fig. 6.

2) Response of Three Categories of Plant Community Temperatures to Extreme Temperatures: For evaluating the response of different plant community categories to extreme

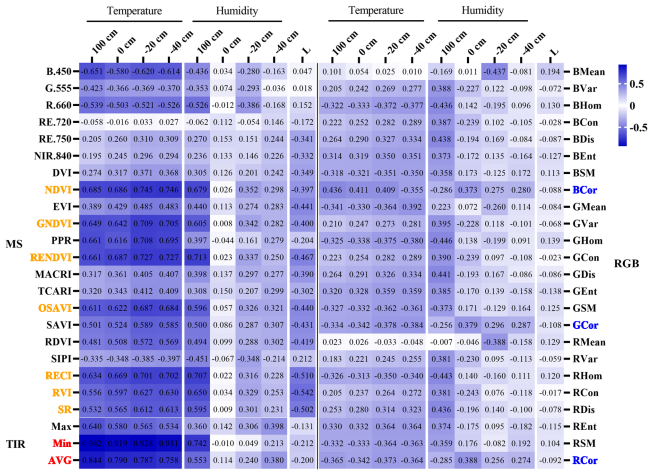

Fig. 7. Pearson correlation coefficients among MS, RGB, and TIR variables and temperature, humidity, and illumination (L). Explanation: orange, red, and blue fonts indicate MS, TIR, and RGB variables with high correlation with environmental data, respectively.

temperatures, special attention was paid to four time periods of drastic temperature changes. Summer high-temperature phases: 11/08/2022–18/08/2022 and 20/06/2023–27/06/2023; and winter low-temperature phases: 28/11/2022–05/12/2023 and 11/03/2023–18/03/2023. The maximum (Max-) and minimum (Min-) temperature variations in the 0 cm of the C1, C2, and C3 plant communities were analyzed [see Fig. 5(b)]. It can be noticed that, during the high-temperature phase, the temperature of C1 was always higher than that of C2 and C3, and C2 and C3 exhibited a good buffering capacity. For instance, for the maximum temperature on 15 August 2022, C2 and C3 were 0.4 °C and 2.7 °C lower than C1, respectively. During the low-temperature phase, the temperature of C1 was always lower than that of C2 and C3, and C2 and C3 exhibited good thermal insulation. For example, for the minimum temperature on 1 December 2022, C2 and C3 were 0.9 °C and 1.5 °C higher than C1, respectively. Overall, compared with C1, the rich vegetation of C2 and C3 created a localized climatic environment with warmer winters and cooler summers for the tea plant. The C2 and C3 had favorable stability to maintain lower temperatures during summer warming and higher temperatures during winter cooling.

B. Construction and Fitting of NTEIs

1) Correlation Analysis of Remote Sensing Variables and Environmental Data: A total of 48 remote sensing variables were obtained from MS, RGB, and TIR images. To determine the remote sensing variables that were sensitive to environmental changes, the correlations between the 48 remote sensing variables and the temperature, humidity, and illumination data of the plant community were analyzed. The Pearson correlation coefficient matrix is shown in Fig. 7. The results demonstrated that the correlation between remote sensing variables and temperature data was higher than that with illuminance and humidity data. The correlation between illuminance data and MS variables was

TABLE V
EIGENVALUES AND VCS OF CORRELATION MATRICES OF REMOTE SENSING VARIABLES

Component (Y)	λ	VC (%)	CVC (%)
1	6.969	58.076	58.076
2	3.206	26.719	84.795
3	1.236	10.302	95.098
4	0.251	2.095	97.192
5	0.145	1.207	98.399
6	0.122	1.020	99.420
7	0.033	0.273	99.692
8	0.025	0.210	99.902
9	0.006	0.046	99.948
10	0.003	0.027	99.975
11	0.002	0.014	99.989
12	0.001	0.011	100.000

TABLE VI
PRINCIPAL COMPONENT LOADINGS FOR 12 REMOTE SENSING VARIABLES

	Y_1	Y_2	Y_3
NDVI (X_1)	0.966	0.016	−0.052
GNDVI (X_2)	0.968	0.058	−0.100
RECI (X_3)	0.976	−0.011	−0.080
RENDVI (X_4)	0.955	0.095	−0.066
OSAVI (X_5)	0.967	−0.003	−0.112
RVI (X_6)	0.926	0.101	−0.169
SR (X_7)	0.938	0.110	−0.219
BCor (X_8)	0.007	0.983	0.181
GCor (X_9)	0.042	0.982	0.175
RCor (X_{10})	−0.017	0.977	0.205
Min (X_{11})	0.514	−0.479	0.659
AVG (X_{12})	0.542	−0.239	0.764

higher; and the correlation between temperature and humidity data and TIR variables was higher, followed by MS variables and RGB variables. For TIR variables, Min and AVG showed a high correlation with temperature and humidity. The correlation coefficient of Min with 100 cm temperature was as high as 0.942. For MS variables, NDVI, green-normalized difference vegetation index (GNDVI), red-edge NDVI (RENDVI), optimization of soil-adjusted vegetation index (OSAVI), red-edge chlorophyll index (RECI), ratio vegetation index (RVI), and simple ratio (SR) vegetation index exhibited a higher correlation with temperature, humidity, and illuminance. Especially, the correlation with temperature data was stronger, with correlation coefficients greater than 0.530. For RGB variables, blue correlation (BCor), green correlation (GCor), and red correlation (RCor) displayed higher correlations with temperature and humidity. Similarly, they showed a higher correlation with temperature data compared with humidity and illuminance data. Therefore, 12 remote sensing variables highly correlated with temperature, humidity, and illumination data were selected to participate in the construction of the NTEI, including TIR variables (Min and AVG), MS variables (NDVI, GNDVI, RENDVI, OSAVI, RECI, RVI, and SR), and RGB variables (BCor, GCor, and RCor).

2) Construction of NTEI Based on Highly Correlated Remote Sensing Variables: In order to comprehensively analyze the stability of different plant communities in response to weather conditions change, 12 remote sensing variables were assembled into NTEI using PCA. To avoid the weight imbalance caused by dimensional inconsistency, the 12 remote sensing variables were first standardized before the PCA operation. Subsequently, PCA operations were performed (see Tables V and VI). The data in Table V indicated that the eigenvalues (λ) of the first three principal components (Y_1, Y_2, and Y_3) were all greater than 1, and their cumulative contribution was as high as 95.098%. The Y_1, Y_2, and Y_3 were able to respond to most of the information of the 12 remote sensing variables. Therefore, Y_1, Y_2, and Y_3 were utilized to construct NTEI.

Based on the data in Tables V and VI, the *LCC* was calculated using (1) to yield linear composite expressions for Y_1, Y_2, and Y_3

$$\begin{aligned} Y_1 = {} & 0.366X_1 + 0.367X_2 + 0.370X_3 + 0.362X_4 + 0.366X_5 \\ & + 0.351X_6 + 0.355X_7 + 0.003X_8 + 0.016X_9 \\ & - 0.007X_{10} + 0.195X_{11} + 0.205X_{12} \end{aligned} \tag{9}$$

$$\begin{aligned} Y_2 = {} & 0.009X_1 + 0.032X_2 - 0.006X_3 + 0.053X_4 - 0.002X_5 \\ & + 0.056X_6 + 0.062X_7 + 0.549X_8 + 0.548X_9 \\ & + 0.546X_{10} - 0.267X_{11} - 0.133X_{12} \end{aligned} \tag{10}$$

$$\begin{aligned} Y_3 = {} & - 0.047X_1 - 0.090X_2 - 0.072X_3 - 0.059X_4 \\ & - 0.101X_5 - 0.1524X_6 - 0.197X_7 + 0.163X_8 \\ & + 0.158X_9 + 0.184X_{10} + 0.593X_{11} + 0.687X_{12}. \end{aligned} \tag{11}$$

After that, the CSC was calculated using (2) to obtain the formula for the principal component (Y)

$$\begin{aligned} Y = {} & 0.221X_1 + 0.223X_2 + 0.216X_3 + 0.229X_4 + 0.212X_5 \\ & + 0.214X_6 + 0.213X_7 + 0.174X_8 + 0.181X_9 \\ & + 0.169X_{10} + 0.108X_{11} + 0.162X_{12}. \end{aligned} \tag{12}$$

Finally, the percentage-based approach was normalized for each coefficient of the Y-equation. The final equation for NTEI was obtained as follows:

$$\begin{aligned} \mathrm{NTEI} = {} & 0.095X_1 + 0.096X_2 + 0.093X_3 + 0.099X_4 \\ & + 0.091X_5 + 0.092X_6 + 0.092X_7 + 0.075X_8 \\ & + 0.078X_9 + 0.073X_{10} + 0.047X_{11} + 0.070X_{12}. \end{aligned} \tag{13}$$

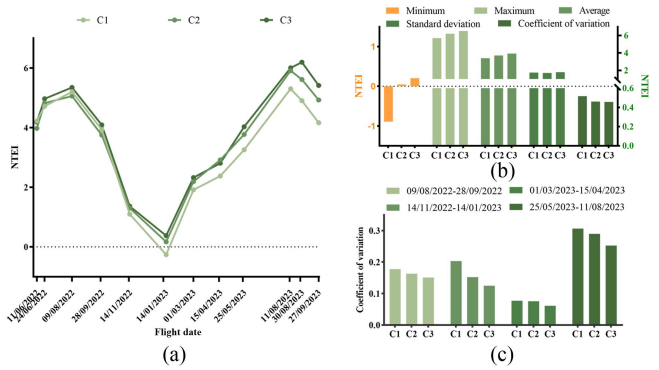

Fig. 8. Analysis of NTEI for three categories of plant communities. (a) Temporal variation curves of NTEI. (b) Descriptive statistics of NTEI. (c) Comparison of CV of NTEI.

C. NTEI Analysis of Different Categories of Plant Communities

The characteristics of temporal variation in NTEI: In the context of the NTEI formula, the theoretical value range of NTEI is [−3, 9]. However, it is worth noting that this range is not an absolute theoretical range, but a relative range. In order to elucidate the ecological meaning of NTEI, the seasonal variation characteristics of NTEI in different plant communities were analyzed. Fig. 8 displays the variation curves of NTEI, ranging from −0.890 to 6.526. From a temporal perspective, the period from July to September of each year is observed to be at the peak of the overall trend. For example, during the observation on 30/08/2023, the NTEI values for C1, C2, and C3 were 4.906, 5.616, and 6.197, respectively, exhibiting a significant decreasing trend. The period from January to February 2023 represented the low peak of the overall trend. At the lowest point on 14/1/2023, the NTEI values for C1, C2, and C3 were −0.259, 0.171, and 0.378, in which order again confirmed that the NTEI value of C3 was higher than those of C2 and C1. This phenomenon clearly indicates that communities with higher coverage tend to have higher NTEI values. It is particularly noteworthy that this trend of high and low peaks coincided with the actual temperature variation curves in Fig. 5(a). For instance, the reason for the lowest peak may be related to the winter season, which leads to a decrease in air and soil temperatures, a reduction in water vapor content, as well as a decline in the coverage area of surface vegetation. Overall, the variation curve of NTEI exhibited significant seasonality, gradually decreasing with the transition from midsummer (June–September) to severe winter (November–February), and increasing with the alternation of winter and summer, demonstrating a cyclical pattern of change. More importantly, the performance of NTEI was close to actual conditions, demonstrating significant interannual variations that are consistent with the actual phenological changes of deciduous trees in the north. Therefore, the magnitude of NTEI values indeed provides us with important information regarding the degree of vegetation coverage. The higher the vegetation coverage of the tea plantation community, the larger the NTEI value; the lower the vegetation coverage of the tea plantation community, the smaller the NTEI value.

The statistical analysis of NTEI: Fig. 8 illustrates the statistical analysis of NTEI for three categories of plant communities, including maximum value, minimum value, standard deviation, and coefficient of variation (CV). The data showed that the CV was 0.518, 0.461, and 0.458 for C1, C2, and C3, respectively. The three plant communities were ranked in ascending order of the CV: C3 < C2 < C1. The use of CV values for the plant community helped to elucidate the extent and rate of change in the data and to reflect the discrete and fluctuating the NTEI distribution. If the vegetation characteristics and microclimate of the plant community tend to be stable, then the fluctuation of NTEI will be smaller and the CV value will be lower. On the contrary, if the vegetation characteristics and microclimate of the plant community change drastically, then the fluctuation of NTEI will be greater and the CV value will be larger. Therefore, among the three categories of plant communities, C3 was the most stable and less susceptible to external factors.

The variability analysis of NTEI: To more intuitively identify the differences between different time series and communities, and to further validate the feasibility of NTEI in characterizing plant community stability, the CV value was used to analyze and interpret NTEI under different spatiotemporal conditions. Specifically, the CV of NTEI for four remote sensing fly-testing phases was analyzed. These four remote sensing fly-testing phases were 09/08/2022–28/09/2022, 14/11/2022–14/01/2023, 01/03/2023–15/04/2023, and 25/05/2023–11/08/2023, which encompassed the four time periods of drastic temperature changes in Section III-A. Fig. 8 displayed the comparison results of the CV of the NTEI in the three categories of plant communities, and it can be observed that C1 always has the largest CV, followed by C2, while C3 always has the smallest CV. This is consistent with the differences in the response of the three categories of plant communities to extreme temperatures [see Fig. 5(b)]. The results indicated that NTEI can effectively characterize the buffering effect of plant communities in tea plantations on temperature and the stability of vegetation phenology. Furthermore, during the period from 25/05/2023 to 11/08/2023, the CV values of various communities were particularly large (C1, 0.307; C2, 0.290; and C3, 0.252), indicating significant differences between different communities. Besides the inherent differences among different communities, this may also be attributed to the fact that this period was in the peak growth stage of plants. During this time, the phenotypic changes of vegetation were obvious and significantly influenced by external environmental factors. Therefore, this period serves as an excellent phase for studying the diversity of plant communities in northern tea plantations.

D. Quantization of NTEI Curves

To compensate for the lack of remote sensing data during the study period and to promote the application of remote sensing data for multitemporal ecological analyses, the NTEI data were fitted using the Fourier function (3). Table VII lists the coefficients and fitting efficacies of the equations of the fitted curves for the NTEI of the nine plant communities. The results indicated that the trend of the NTEI fitted curve based on the

TABLE VII
PARAMETERS OF NTEI FITTING CURVES FOR DIFFERENT PLANT COMMUNITIES

NO.	Coefficients (with 95% confidence bounds)				Goodness of fit			
	a_0	a	w	b	R^2	Adj.R^2	SSE	RMSE
1	2.300 (±0.270)	1.748 (±0.509)	0.0174 (±0.0010)	1.740 (±0.642)	0.842	0.782	5.867	0.856
2	2.880 (±0.250)	1.858 (±0.429)	0.0161 (±0.0012)	1.234 (±0.695)	0.856	0.802	4.996	0.790
3	3.220 (±0.274)	2.080 (±0.447)	0.0162 (±0.0012)	1.129 (±0.782)	0.843	0.783	6.046	0.869
4	3.373 (±0.301)	20157 (±0.420)	0.0138 (±0.0014)	-0.708 (±0.792)	0.847	0.790	5.802	0.852
5	3.097 (±0.278)	2.148 (±0.441)	0.0161 (±0.0013)	1.151 (±0.815)	0.840	0.780	6.660	0.912
6	3.028 (±0.220)	1.825 (±0.380)	0.0164 (±0.0010)	1.223 (±0.604)	0.874	0.827	3.944	0.702
7	3.368 (±0.211)	1.979 (±0.369)	0.0160 (±0.0010)	1.394 (±0.582)	0.910	0.876	3.558	0.667
8	2.834 (±0.198)	2.227 (±0.316)	0.0161 (±0.0009)	1.137 (±0.578)	0.921	0.891	3.149	0.627
9	3.058 (±0.182)	2.179 (±0.241)	0.0154 (±0.0009)	0.347 (±0.558)	0.920	0.890	2.534	0.563

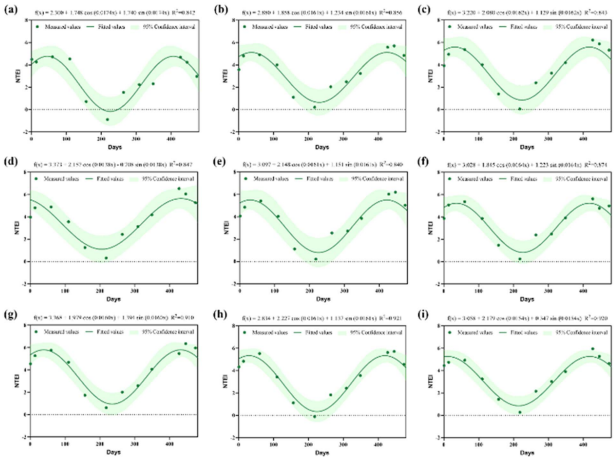

Fig. 9. Fitted curves for different plant communities. (a) NO.1. (b) NO.2. (c) NO.3. (d) NO.4. (e) NO.5. (f) NO.6. (g) NO.7. (h) NO.8. (i) NO.9.

Fourier function was in accordance with the actual value and could accurately fit the annual trend of NTEI. The R^2 between the fitted and actual NTEI values for the nine plant communities was greater than 0.840, and the goodness of fit was as expected from the research. Among them, the best fit to the NTEI data was achieved for NO.8, with R^2, Adj.R^2, SSE, and RMSE of 0.921, 0.891, 3.149, and 0.627, respectively; and the worst fit to the NTEI data was achieved for NO.5, with R^2, Adj.R^2, SSE, and RMSE of 0.840, 0.780, 6.660, and 0.912, respectively. Fig. 9 shows the actual values and the fitted curves of the NTEI. Among the nine fitted curves, the actual NTEI values at x60, x110, x309, and x349 were closest to the fitted values, while the other dates were somewhat overestimation or underestimation. Moreover, the Fourier function is periodic, which fits well with the seasonal cyclic variation pattern of the NTEI.

E. Modeling of NTEI Predictions

Due to the large volume of environmental data, environmental data obtained after long-term monitoring in the form of external factors can accurately reflect the dynamic characteristics of vegetation growth variations. In this study, temperature, humidity, and illuminance data were used as intermediate data, and CNN-GRU, CNN, GRU, and SVM networks were utilized to achieve synergistic transformation between environmental data and NTEI data, and ultimately the prediction of NTEI data. Table VIII lists the prediction performance of the models. The data indicated that CNN-GRU, CNN, GRU, and SVM were able to achieve the expected results in predicting NTEI ($Rp^2 > 0.888$). Specifically, compared with the single model CNN, GRU, and the machine learning model SVM, the CNN-GRU had the best prediction accuracy, with Rp^2 and RMSEP of 0.955 and 0.314, respectively. Fig. 10 shows the scatter plot of the actual and predicted values of NTEI. The black diagonal line indicated the 1:1 line, and the orange dashed line indicated the regression line between the predicted values and the actual values. The predicted values of NTEI have all been distributed around the regression line at a closer distance, which indicates that the four models have good robustness.

TABLE VIII
PREDICTIVE PERFORMANCE OF CNN-GRU, CNN, GRU, AND SVM

Model	Rc^2	RMSEC	RMSECV	Rp^2	RMSEP
CNN-GRU	0.960	0.314	0.497	0.955	0.314
CNN	0.947	0.323	0.519	0.945	0.324
GRU	0.957	0.320	0.380	0.888	0.566
SVM	0.934	0.433	0.514	0.924	0.465

IV. DISCUSSION

A. Feasibility of NTEI Application for Ecological Monitoring of Tea Plantations

Remote sensing technology is widely used in ecological environment monitoring and evaluation by scholars in various countries because of its macroscopic, real-time, rapid, dynamic, and objective features [33]. With the prevalence of RSEI, it can reasonably respond to the ecological status of a region, and has been well applied to many regions [4], [34]. However, more and more scholars have discussed that the ecological environments

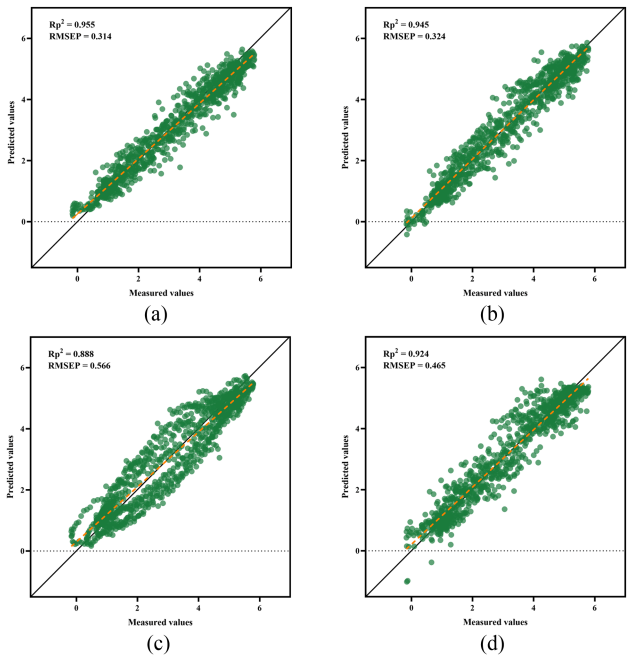

Fig. 10. Scatter plot of actual and predicted NTEI values. (a) CNN-GRU. (b) CNN. (c) GRU. (d) SVM.

in different areas are regionally characterized and that relying only on RSEI for ecological assessment is not very representative [35], [36], [37]. Therefore, it is necessary to improve or establish new remote sensing indicators for specific regions. From the perspective of sensor types, this work identified 12 remote sensing variables that are highly correlated with regional environmental parameters to construct the NTEI. The NTEI effectively integrated the effective information of spectral index, texture features, and heat. The index's indicator system took into account the influence of multiple factors, such as temperature, humidity, heat, vegetation, and soil, on the ecological status of tea plantations, making it more suitable for ecological monitoring of tea plantations over long time periods and multiple types. This overcame the limitations of the ecological status evaluation method based on only one indicator, especially in the comprehensive reaction to the overall status of complex ecosystems [38]. In addition, the construction of NTEI was coupled with the indicators through PCA, which avoided the errors caused by artificially setting the weights and thresholds, and made the results objective and stabilized. This process is the same as the process of constructing RSEI by Xu [39].

The application of NTEI in the Chunxi Tea Plantation demonstrated that the seasonal variations of NTEI were consistent with the variations of temperature and vegetation phenology characteristics (see Fig. 5). Consequently, the NTEI can be used to delicately characterize the ecological condition of the tea plantation and the regional environmental condition. The higher the vegetation coverage, the larger the NTEI; and conversely, the smaller the NTEI. The relevant results of this study proved that the NTEI is a novel and powerful indicator that can be utilized to quantify and monitor the ecological status of tea plantations at small scales, and thereby facilitate the practical application of monitoring the status of different ecological tea plantations.

However, it is worth noting that, in complex ecosystems, changes in meteorological conditions (such as temperature and humidity) often have a certain time-lag effect on remote sensing variables, such as vegetation spectral characteristics [40]. Specifically, the overall low correlation (see Fig. 7) observed in this study between remote sensing variables and temperature, humidity, and illumination data may be a manifestation of this lag effect. Therefore, to gain a deeper insight into this phenomenon, it is necessary to use the longer time series of basic data to investigate the time-lag effect of remote sensing variables in response to changes in weather conditions. Concurrently, the new generation artificial intelligence technologies will be employed to explore key features and optimize parameters, such as time lag and sensitivity factors. This approach will enhance the correlation between environmental parameters and remote sensing variables, thereby ensuring the timely representation of tea plantation ecological effectiveness by NTEI.

B. Plant Diversity Contributes to the Stability of Ecological Tea Plantations

The vegetation is strongly related to the surrounding environment and is very sensitive to changes in the ecological environment. The changes in the regional ecological environment are often hypothesized according to the stability characteristics of the vegetation itself and the regularity of response to the changes in the external environment. The ecological variability is measured by CV. The CV indicates the proportion of variation around the mean value. The lower the stability, the higher this value [41]. Tilman et al. [42], [43] studied biomass changes in 207 grasslands with different levels of diversity and pointed out that diversity promotes community stability (lower CV). In this study, three plant communities with species richness levels were set up, including C1, C2, and C3 (see Fig. 2). Based on the NTEI to assess the ecological feasibility of the tea plantation, the stability of the three plant communities was evaluated using the CV values of the NTEI. The results revealed that the C3 with higher vegetation density exhibited smaller fluctuations (lower CV) (see Fig. 8). This suggested that plant diversity contributes to the stability of ecosystems. This result is in accordance with the conclusion obtained by Wu et al. [44] in their study on the impact of diversity on stability based on NDVI.

Some studies, however, have also found a negative correlation between ecological stability and plant diversity in certain environments, especially in redundant states where species abundance reaches saturation point [45]. Accordingly, in an effort to more scientifically explore the relationship between plant diversity and ecological stability in ecological tea plantations, it is imperative to conduct investigations and studies in tea plantations with more levels of diversity in the future. Finding the saturation point where plant diversity increases ecosystem stability and providing a theoretical basis for the scientific construction of ecological tea plantations with high stability.

C. Robustness of Hybrid Deep Learning Networks

With the advancement of machine learning, the research on remote sensing image inversion has made rapid progress [46]. Traditional machine learning algorithms, such as SVM, PLS, and RF, have been widely applied to agricultural remote sensing parsing research [47], [48]. In recent years, deep learning has become an emerging research direction in the field of machine learning [49]. One of our recent studies has shown that the CNN-GRU network exhibits a better fitting ability when dealing with 160 data related to tea plant freeze damage, and the Rp^2 of the optimal model was 0.850 [19]. In exploring the performance of hybrid networks, such as CNN-GRU and CNN-LSTM, Yu et al. [50] proposed to further enrich the amount of data used for model training and improve the accuracy of the models. Furthermore, this study explored the robustness of hybrid deep learning networks with respect to massive remote sensing data by utilizing CNN-GRU. According to the prediction results of NTEI, the CNN-GRU ($Rp^2 = 0.955$) outperforms the independent CNN, GRU model, and traditional SVM model in terms of prediction accuracy (see Table VIII). This result suggested that the combination of CNNs feature extraction capability and GRUs temporal memory capability improved the predictive performance of the model. This is attributed to the large training sample (2821) of this study. In addition, Fourier functions are characterized by universality and the fact that they work best in describing periodic functions [51]. The Fourier function fitting method was utilized to quantify daily NTEI data. This has made an essential contribution to obtaining continuous time series of NTEI data as well as large datasets.

V. Conclusion

Basis on full consideration of plant communities and weather conditions' characteristics, 12 remote sensing variables were selected to construct NTEI, and the Fourier function was used to fit the daily variation curves of the NTEI; finally, a prediction model of NTEI based on the environmental data was constructed using CNN-GRU, CNN, GRU, and SVM. The results indicated that NTEI has the potential to monitor the ecology of tea plantations and its variations in the case of the Chunxi Tea Plantation. The main conclusions of this study are given as follows.

1) The NTEI enables a delicate characterization of the ecological status of tea gardens, and its variation is consistent with changes in temperature and vegetation phenology.
2) The Fourier function allows for the accurate quantification of the daily variation in NTEI, with a fitted R^2 above 0.840.
3) Compared with CNN, GRU, and SVM models, the CNN-GRU is more appropriate for predicting long-term NTEI and has the best prediction performance ($Rp^2 = 0.955$ and RMSEP = 0.314).
4) Plant diversity contributes to ecosystem stability, with high-density C3 plant communities having the ability to buffer high/low temperatures and C3 having the smallest NTEI variance (C1's CV = 0.518; C2's CV = 0.461; C3's CV = 0.458).

The establishment and application of NTEI in the ecological monitoring and assessment of Chunxi Tea Plantation demonstrated the enormous potential of synergizing environmental parameters with multisource remote sensing data, as well as the significant advantages of cascade application of the Fourier fitting model and NTEI-CNN-GRU model. This provides a novel strategy for rapidly assessing the plant community of tea plantations and a new idea for the scientific construction of ecological tea plantations. In the future, on the one hand, tests should be conducted in tea plantations with various complex structures and environmental conditions to further validate the robustness and generalizability of the NTEI-CNN-GRU model in evaluating the ecological aspects of tea plantations. On the other hand, emphasis should be placed on acquiring and analyzing the ecological indicators (biomass and quality) of tea plants and integrating them with the NTEI model to further reveal the ecological value of NTEI for the tea plantation. This will facilitate a deeper understanding of the role of NTEI in the tea plantation ecosystem and enhance the interpretability of the model.

References

[1] C. Wang, M. Zhao, Y. Xu, Y. Zhao, and X. Zhang, "Ecosystem service synergies promote ecological tea gardens: A case study in Fuzhou, China," *Remote Sens.*, vol. 15, no. 2, 2023, Art. no. 540.
[2] X. Lei et al., "Progress and perspective on intercropping patterns in tea plantations," *Beverage Plant Res.*, vol. 2, no. 1, 2022, Art. no. 18.
[3] H. Moller, F. Berkes, P. O. B. Lyver, and M. Kislalioglu, "Combining science and traditional ecological knowledge: Monitoring populations for co-management," *Ecol. Soc.*, vol. 9, no. 3, 2004, Art. no. 2.
[4] E. K. Melaas, M. A. Friedl, and Z. Zhu, "Detecting interannual variation in deciduous broadleaf forest phenology using Landsat TM/ETM+ data," *Remote Sens. Environ.*, vol. 132, pp. 176–185, 2013.
[5] H. Xu, Y. Wang, H. Guan, T. Shi, and X. Hu, "Detecting ecological changes with a remote sensing based ecological index (RSEI) produced time series and change vector analysis," *Remote Sens.*, vol. 11, no. 20, 2019, Art. no. 2345.
[6] T. V. Bijeesh and K. N. Narasimhamurthy, "A comparative study of spectral indices for surface water delineation using Landsat 8 images," in *Proc. Int. Conf. Data Sci. Commun.*, Bangalore, India, 2019, pp. 1–5.
[7] S. Khare, H. Latifi, and S. Khare, "Vegetation growth analysis of UNESCO world heritage Hyrcanian forests using multi-sensor optical remote sensing data," *Remote Sens.*, vol. 13, no. 19, 2021, Art. no. 3965.
[8] W. Zhang et al., "Remotely sensing the ecological influences of ditches in Zoige Peatland, eastern Tibetan Plateau," *Int. J. Remote Sens.*, vol. 35, no. 13, pp. 5186–5197, 2014.
[9] M. S. Boori, K. Choudhary, R. Paringer, and A. Kupriyanov, "Spatiotemporal ecological vulnerability analysis with statistical correlation based on satellite remote sensing in Samara, Russia," *J. Environ. Manage.*, vol. 285, 2021, Art. no. 112138.
[10] M. Guo and S. Wang, "Remote sensing monitoring and ecological risk assessment of landscape patterning in the agro-pastoral ecotone of Northeast China," *Complexity*, vol. 2021, 2021, Art. no. 8851543.
[11] Z. Zheng et al., "Mapping functional diversity using individual tree-based morphological and physiological traits in a subtropical forest," *Remote Sens. Environ.*, vol. 252, 2020, Art. no. 112170.
[12] M. L. Salandra, R. Roseto, D. Mele, P. Dellino, and D. Capolongo, "Probabilistic hydro-geomorphological hazard assessment based on UAV-derived high-resolution topographic data: The case of Basento river (Southern Italy)," *Sci. Total Environ.*, vol. 842, 2022, Art. no. 156736.
[13] Y. Shi et al., "Using unmanned aerial vehicle-based multispectral image data to monitor the growth of intercropping crops in tea plantation," *Front. Plant Sci.*, vol. 13, 2022, Art. no. 820585.
[14] H. Li, Y. Wang, K. Fan, Y. Mao, Y. Shen, and Z. Ding, "Evaluation of important phenotypic parameters of tea plantations using multi-source remote sensing data," *Front. Plant Sci.*, vol. 13, 2022, Art. no. 898962.
[15] D. Luo et al., "Using UAV image data to monitor the effects of different nitrogen application rates on tea quality," *J. Sci. Food Agriculture*, vol. 102, no. 4, pp. 1540–1549, 2022.

[16] S. Zhong, Z. Sun, and L. Di, "Characteristics of vegetation response to drought in the CONUS based on long-term remote sensing and meteorological data," *Ecol. Indicators*, vol. 127, 2021, Art. no. 107767.
[17] P. Leng, Z.-L. Li, S.-B. Duan, M.-F. Gao, and H.-Y. Huo, "A practical approach for deriving all-weather soil moisture content using combined satellite and meteorological data," *ISPRS J. Photogramm. Remote Sens.*, vol. 131, pp. 40–51, 2017.
[18] H. Li et al., "Environmental simulation model for rapid prediction of tea seedling growth," *Agronomy*, vol. 12, no. 12, 2022, Art. no. 3165.
[19] Y. Mao et al., "Rapid monitoring of tea plants under cold stress based on UAV multi-sensor data," *Comput. Electron. Agriculture*, vol. 213, 2023, Art. no. 108176.
[20] H. Naito et al., "Estimating rice yield related traits and quantitative trait loci analysis under different nitrogen treatments using a simple tower-based field phenotyping system with modified single-lens reflex cameras," *ISPRS J. Photogramm. Remote Sens.*, vol. 125, pp. 50–62, 2017.
[21] C. J. Tucker, "Red and photographic infrared linear combinations for monitoring vegetation," *Remote Sens. Environ.*, vol. 8, no. 2, pp. 127–150, 1979.
[22] R. B. Gurung, F. J. Breidt, A. Dutin, and S. M. Ogle, "Predicting enhanced vegetation index (EVI) curves for ecosystem modeling applications," *Remote Sens. Environ.*, vol. 113, no. 10, pp. 2186–2193, 2009.
[23] A. A. Gitelson, Y. J. Kaufman, and M. N. Merzlyak, "Use of a green channel in remote sensing of global vegetation from EOS-MODIS," *Remote Sens. Environ.*, vol. 58, no. 3, pp. 289–298, 1996.
[24] G. Metternicht, "Vegetation indices derived from high-resolution airborne videography for precision crop management," *Int. J. Remote Sens.*, vol. 24, no. 14, pp. 2855–2877, 2003.
[25] J. Penuelas, B. Frederic, and I. Filella, "Semi-empirical indices to assess carotenoids/chlorophyll—A ratio from leaf spectral reflectances," *Photosynthetica*, vol. 31, no. 2, pp. 221–230, 1995.
[26] Y. Kanke, B. Tubana, M. Dalen, and D. Harrell, "Evaluation of red and red-edge reflectance-based vegetation indices for rice biomass and grain yield prediction models in paddy fields," *Precis. Agriculture*, vol. 17, no. 5, pp. 507–530, 2016.
[27] P. J. Zarco-Tejada, J. R. Miller, A. Morales, A. Berjón, and J. Agüera, "Hyperspectral indices and model simulation for chlorophyll estimation in open-canopy tree crops," *Remote Sens. Environ.*, vol. 90, no. 4, pp. 463–476, 2004.
[28] G. Rondeaux, M. Steven, and F. Baret, "Optimization of soil-adjusted vegetation indices," *Remote Sens. Environ.*, vol. 55, no. 2, pp. 95–107, 1996.
[29] A. R. Huete, "A soil-adjusted vegetation index (SAVI)," *Remote Sens. Environ.*, vol. 25, no. 3, pp. 295–309, Aug. 1988.
[30] G. Melillos and D. G. Hadjimitsis, "Using simple ratio (SR) vegetation index to detect deep man-made infrastructures in Cyprus," *SPIE-Detection Sens. Mines, Explosive Objects, Obscured Targets*, vol. 11418, pp. 105–113, 2020.
[31] R. M. Haralick, K. Shanmugam, and I. H. Dinstein, "Textural features for image classification," *IEEE Trans. Syst., Man, Cybern.*, vol. SMC-3, no. 6, pp. 610–621, Nov. 1973.
[32] Y. Mao et al., "Low temperature response index for monitoring freezing injury of tea plant," *Front. Plant Sci.*, vol. 14, 2023, Art. no. 1096490.
[33] Jing Zhang, J. Zhang, X. Du, K. Hou, and M. Qiao, "An overview of ecological monitoring based on geographic information system (GIS) and remote sensing (RS) technology in China," *IOP Conf. Ser., Earth Environ. Sci.*, vol. 94, no. 1, 2017, Art. no. 012056.
[34] Y. Xiong et al., "Assessment of spatial–temporal changes of ecological environment quality based on RSEI and GEE: A case study in Erhai Lake Basin, Yunnan province, China," *Ecol. Indicators*, vol. 125, 2021, Art. no. 107518.
[35] D. Zhu, T. Chen, Z. Wang, and R. Niu, "Detecting ecological spatial-temporal changes by remote sensing ecological index with local adaptability," *J. Environ. Manage.*, vol. 299, 2021, Art. no. 113655.
[36] H. Wu et al., "A novel remote sensing ecological vulnerability index on large scale: A case study of the China-Pakistan economic corridor region," *Ecol. Indicators*, vol. 129, 2021, Art. no. 107955.
[37] D. Zhu, T. Chen, N. Ruiqing, and Z. Na, "Ecological environment assessment of mining area by using moving window-based remote sensing ecological index," in *Proc. IEEE Int. Geosci. Remote Sens. Symp.*, Yokohama, Japan, 2019, pp. 9942–9945.
[38] L. Jiang, Y. Liu, S. Wu, and C. Yang, "Analyzing ecological environment change and associated driving factors in China based on NDVI time series data," *Ecol. Indicators*, vol. 129, 2021, Art. no. 107933.
[39] H.-Q. Xu, "A remote sensing urban ecological index and its application," *Acta Ecologica Sinica*, vol. 33, no. 24, pp. 7853–7862, 2013.
[40] T. Wu, F. Feng, Q. Lin, and H. Bai, "Advanced method to capture the time-lag effects between annual NDVI and precipitation variation using RNN in the arid and semi-arid grasslands," *Water*, vol. 11, no. 9, 2019, Art. no. 1789.
[41] D. Tilman, C. L. Lehman, and C. E. Bristow, "Diversity-stability relationships: Statistical inevitability or ecological consequence?," *Amer. Naturalist*, vol. 151, no. 3, pp. 277–282, 1998.
[42] D. Tilman, "Biodiversity: Population versus ecosystem stability," *Ecology*, vol. 77, no. 2, pp. 350–363, 1996.
[43] D. Tilman, P. B. Reich, and J. M. Knops, "Biodiversity and ecosystem stability in a decade-long grassland experiment," *Nature*, vol. 441, no. 7093, pp. 629–632, 2006.
[44] L. Wu et al., "Soil biota diversity and plant diversity both contributed to ecosystem stability in grasslands," *Ecol. Lett.*, vol. 26, no. 6, pp. 858–868, 2023.
[45] T. Tscharntke, A. M. Klein, A. Kruess, I. Steffan-Dewenter, and C. Thies, "Landscape perspectives on agricultural intensification and biodiversity–ecosystem service management," *Ecol. Lett.*, vol. 8, no. 8, pp. 857–874, 2005.
[46] Y. Tian et al., "Aboveground mangrove biomass estimation in Beibu Gulf using machine learning and UAV remote sensing," *Sci. Total Environ.*, vol. 781, 2021, Art. no. 146816.
[47] A. M. Ali, R. Darvishzadeh, A. Skidmore, T. W. Gara, and M. Heurich, "Machine learning methods' performance in radiative transfer model inversion to retrieve plant traits from Sentinel-2 data of a mixed mountain forest," *Int. J. Digit. Earth*, vol. 14, no. 1, pp. 106–120, 2021.
[48] K. G. Liakos, P. Busato, D. Moshou, S. Pearson, and D. Bochtis, "Machine learning in agriculture: A review," *Sensors*, vol. 18, no. 8, 2018, Art. no. 2674.
[49] Y. Chen, L. Huang, X. Xie, Z. Liu, and J. Hu, "Improved prediction of hourly PM2.5 concentrations with a long short-term memory and spatio-temporal causal convolutional network deep learning model," *Sci. Total Environ.*, vol. 912, 2024, Art. no. 168672.
[50] J. Yu, X. Zhang, L. Xu, J. Dong, and L. Zhangzhong, "A hybrid CNN-GRU model for predicting soil moisture in maize root zone," *Agricultural Water Manage.*, vol. 245, 2021, Art. no. 106649.
[51] E. B. Brooks, V. A. Thomas, R. H. Wynne, and J. W. Coulston, "Fitting the multitemporal curve: A Fourier series approach to the missing data problem in remote sensing analysis," *IEEE Trans. Geosci. Remote Sens.*, vol. 50, no. 9, pp. 3340–3353, Sep. 2012.

Yilin Mao received the M.S. degree in agriculture from the College of Horticulture, Qingdao Agricultural University, Qingdao, China, in 2024.

She currently conducts research with Tea Research Institute, Shandong Academy of Agricultural Sciences, Jinan, China. Her research interests include tea plant breeding, ecological tea plantations, and multisource remote sensing fusion.

He Li received the M.S. degree in agriculture from the College of Horticulture, Qingdao Agricultural University, Qingdao, China, in 2023. He is currently working toward the Ph.D. degree in seed science and technology with China Agricultural University, Beijing, China.

He conducts research with Tea Research Institute, Shandong Academy of Agricultural Sciences, Jinan, China. His research interests include nondestructive testing and phenomics technology.

Yu Wang received the M.S. degree in horticulture from Shandong Agricultural University, Tai'an, China, in 2005. She is a breeding expert of Taishan Scholars Innovation Team in tea science with Qingdao Agricultural University, Qingdao, China, and a member of Tea Innovation Team Breeding and Cultivation Position of Modern Agricultural Industrial Technology System of Shandong Province.

She has presided more than 20 scientific research projects, including the National Natural Science Foundation of China's general projects. She has participated in the breeding of five new varieties of tea plant. Her main research interests include breeding and cold resistance mechanism of tea plant. She currently conducts research with Tea Research Institute, Shandong Academy of Agricultural Sciences, Jinan, China. Her research interests include tea plant breeding, ecological tea plantations, and multisource remote sensing fusion.

Yang Xu received the B.S. degree in agriculture in 2018 from Qingdao Agricultural University, Qingdao, China, where he is currently working toward the M.S. degree in agronomy and seed industry with the College of Horticulture.

His research interest is in the direction of agricultural informatization, which mainly includes the fusion of remote sensing data, nondestructive detection of pests and diseases in tea plants, and simulation of morphological structures of tea plants.

Kai Fan was born in 1986. He received the Ph.D. degree in tea science from Zhejiang University, Hangzhou, China, in 2016.

He is currently a Lecturer with Qingdao Agricultural University, Qingdao, China. His research interests include the research on the identification of high-quality and resistance phenotypes and digital cultivation of tea plant.

Jiazhi Shen was born in 1990. She received the Ph.D. degree in tea science from Nanjing Agricultural University, Nanjing, China, in 2020.

She is currently an Assistant Research Fellow with Tea Research Institute, Shandong Academy of Agricultural Sciences, Jinan, China. Her main research interests include ecological breeding, drought resistance response mechanisms, and stress resistance phenotype omics of tea plants.

Xiao Han received the M.S. degree in agriculture from the College of Horticulture, Qingdao Agricultural University, Qingdao, China, in 2024.

Her main research interests include cultivation and resistance response mechanism for frost damage recovery of tea plants.

Qingping Ma was born in 1990. She received the Ph.D. degree in tea science from Nanjing Agricultural University, Nanjing, China, in 2019.

She is currently an Associate Professor with the College of Agriculture and Agricultural Engineering, Liaocheng University, Liaocheng, China. Her main research focuses on tea garden ecology and the mechanism of tea plant quality formation.

Hongtao Shi received the Ph.D. degree in computer and technology from the Ocean University of China, Qingdao, China, in 2018.

He currently works with the School of Science and Information Science, Qingdao Agricultural University, Qingdao, China. His main research interests include deep learning algorithm and plant phenomics.

Caihong Bi received the M.S. degree in tea science from Southwest University, Chongqing, China, in 2007. She is a Senior Agronomist, serves as the Director of Linyi Integrated Experimental Station, Shandong Provincial Tea Industry Technology System, Linyi, China.

She currently works with Linyi Agricultural Technology Extension Center, Linyi, China, mainly engaged in research and promotion of tea cultivation techniques.

Yunlai Feng received the B.S. degree in human resource management from Ocean University of China, Qingdao, China, in 2017.

He is a new-generation farmer who utilizes technology to optimize tea plant cultivation. He currently serves as the General Manager of Chunxi Tea Industry Company Limited, Linyi, China. His main research interests include digital tea garden construction and environmental friendly tea processing and production.

Zhaotang Ding received the Ph.D. degree in tea science from Shandong Agricultural University, Tai'an, China, in 2005.

He is a second-level Professor and a Distinguished Professor of Mount Taishan Scholars. From 2006 to 2023, he was a Professor with the College of Horticulture, Qingdao Agricultural University, China. Since 2019, he has been a part-time Professor and a Doctoral Supervisor with Murdoch University, Murdoch, WA, Australia. He is currently the Chief Expert of Tea Research Institute, Shandong Academy of Agricultural Sciences, Jinan, China. His primary research interest includes the molecular mechanisms underlying the growth, development, and environmental responses of tea plants, with a focus on the molecular mechanisms related to tea quality and stress resistance. He has led and undertaken over 30 projects, including the National Natural Science Foundation of China, the National Science and Technology Support Program, and major technological innovation projects at the provincial level. He has authored or coauthored more than 40 research papers in the areas of his interest and holds more than ten invention patents.

Litao Sun received the Ph.D. degree in tea science from the University of Murdoch, Murdoch, WA, Australia, in 2022.

He is currently an Assistant Research Fellow with Tea Research Institute, Shandong Academy of Agricultural Sciences, Jinan, China. His main research interests include phenomics and ecogenomics of tea plants.